



MIXED CONVECTION HEAT TRANSFER IN TRUNCATED CONE ENCLOSURE AS SOLAR CONTAINER WITH INTERNAL CENTERED TRIANGLE OBSTACLE

Kadhun A. Jehhef¹ and Mohamed A. Siba²

¹ Ph.D., Department of Mechanics, Institute of Technology, Middle Technical University, Iraq. Email: kadhun.audaa@yahoo.com

² Ph.D., Department of Mechanics, Institute of Technology, Middle Technical University, Iraq. Email: Moh_siba@yahoo.com

<http://dx.doi.org/10.30572/2018/kje/090420>

ABSTRACT

In this study, the mixed convection heat transfer of the air inside a truncated cone enclosure with aspect ratio of (0.75, 1.75, 2, 2.45 and 2.65) with centered triangle obstacle height varying by (0, 2.5, 5, 7.5, 10, 12.5 and 20 cm) and the heated wall inclination angles of (20°, 30°, 40°, 50°, 60°), the Richardson number in the range of (7 to 11) was investigated numerically. The results are addressed to automotive a suggested solar container with titled solar collector. The heat transfer from the heat source (inclined solar collector) of the enclosure walls is investigated for mixed convection as interaction of the forced convection flow between the inlet and outlet port in the bottom wall. The parameters of heat source, Reynolds number, obstacle height, enclosure aspect ratio, and left and right walls titled angles are considered in this work. The numerical simulation of the problem is carried out using commercial CFD code. The results are given in terms of the streamlines, isothermal, and the enclosure Nusselt number that characterizes the heat transfer from the heat source and from the interior fluid to the enclosure walls, respectively. The results show that the interaction of the main flow and the flow at the heated walls and the buoyancy force at the heated walls increased by using a triangular obstacle and by increasing the obstacle heights, it increased by 20% when using obstacle at position of (h=5 cm). Also, it is found that the Nu increased with increasing Re and the wall heat flux. The Nu increased with increasing Ri in the case of using (h=0 and 5 cm) but it decreased slightly in the other cases and showed that the minimum value of Nu present at a heated wall inclination of $\theta=50^\circ$ but the maximum value at $\theta=30^\circ$.

KEYWORDS: Mixed convection, truncated cone, triangle obstacle, enclosures.

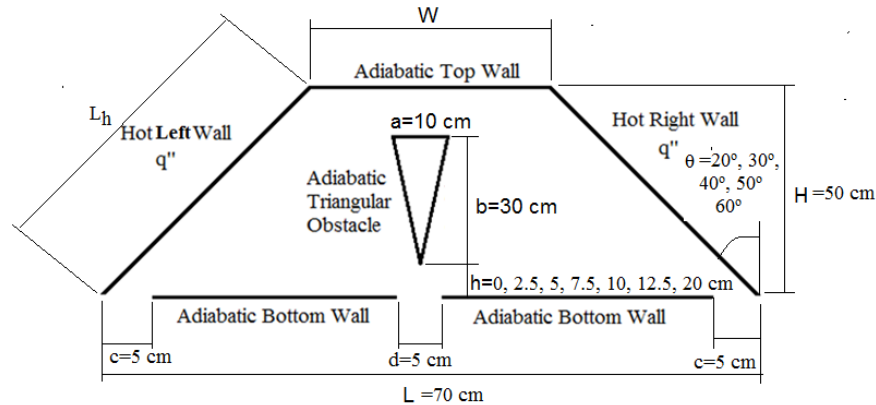
1. INTRODUCTION

The natural convection heat transfer problem in simple geometries enclosures is extensively studied in the previous literatures in the recent years. The most cases are the Rayleigh Bernard cell, vertically heated walls enclosures, and solar container [Sridhar and Reddy, \(2007\)](#). A review of natural convection in cavity with various shapes has been presented in several studies such as (but not limited to) [Wang and Li, \(1999\)](#); [He et al., \(2005\)](#); and [Dixit and Babu, \(2006\)](#). A various shapes as cavities with inclination angles and wavy walls studied by [Aounallah et al., \(2007\)](#), and various trapezoidal cavities presented by [Varol et al., \(2009\)](#). The study of natural convection was presented for triangular enclosures mostly performed by [Fuad et al., \(2007\)](#). [Jan, et al., \(2007\)](#) published a theoretical paper on convective heat transfer in an enclosure with titled wall to study the automotive headlights containing Light Emitting Diodes (LED). They showed that the source convective heat transfer of the wall increases with increasing Reynolds number and also increased with increasing the aspect ratio but it increasing with decreasing the titled angles of the enclosure wall. [Merk and Prins, \(1953\)](#); [Merk and Prins, \(1954\)](#) studied the iso-thermal axi-symmetric forms of the vertical cones and they showed that the vertical cone has such a solution in steady state. Furthermore, [Hossain and Paul , \(2001\)](#) studied the effects of the transpiration velocity on the laminar free convection flow from a vertical non-isothermal cone due to increase the temperature gradient, the velocity and the surface temperature will decrease. [Ramanaiah and Kumaran, \(1992\)](#) have performed an investigated study on...the natural convection about a permeable cone and a cylinder subjected to boundary condition of radiation. [Alamgir, \(1989\)](#) studied the natural convection with laminar flow from vertical cones by using the integral method. [Pop and Takhar, \(1991\)](#) studied the compressibility effects in laminar natural convection from a vertical cone. [Papanicolaou and Jaluria, \(1995\)](#) investigated the effect of varying the position of the heat source inside an enclosure with a constant shape and using a finite thickness of the enclosure sidewalls. [Bapuji, et al., \(2008\)](#) presented a numerical analysis on the natural convection with unsteady laminar flow from an incompressible viscous fluid flows past a vertical cone with uniform surface heat flux. Finally, [Elsayed, et al., \(2016\)](#) studied the effect of heat generation or absorption and thermal radiation on free convection flow and heat transfer over a truncated cone. Comparisons with previously published works, the present study focused on the effect of presence of triangular obstacle inside a truncated cone enclosure with tilted vertical walls on the mixed convection heat transfer coefficients.

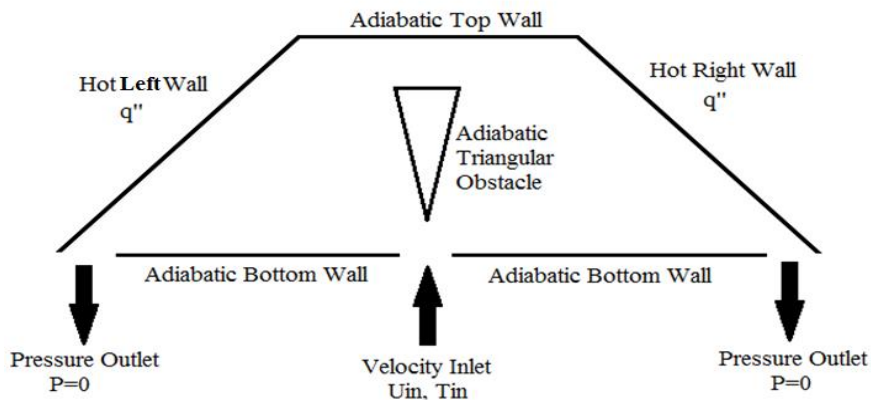
2. NUMERICAL SOLUTION

2.1. Geometry Specification

To study the effect of buoyancy-induced flow regime inside a truncated cone enclosure with heated inclined vertical walls, a two-dimensional physical model and required boundary conditions are displayed in Fig. 1a.



a) Enclosure dimensions



B) Numerical boundary conditions

Fig. 1. Description of problem geometry and boundary conditions.

2.2. Governing Equations

The presentation of the buoyancy-induced regime inside an enclosures performed by the same basic equations of the general fluid motion, namely the conservation of mass, momentum, and energy. The free convection heat transfer scenarios require at least one fluid parameter, density, to vary within the domain of interest. The equation of the buoyancy-induced flows inside a vertical truncated cone for incompressible flow presented by Ganguli et al., (2009):

$$\frac{d\rho}{dt} + \nabla \cdot (\rho \vec{v}) = 0 \quad 1$$

$$\frac{d}{dt} (\rho \cdot \vec{v}) + \nabla \cdot (\rho \vec{v} \vec{v}) = -\nabla P + \nabla \cdot \vec{\tau} + \rho \vec{g} \quad 2$$

$$\frac{d}{dt}(\rho \cdot \vec{T}) + \nabla \cdot (\rho c_p \vec{v} \vec{T}) = \nabla \cdot [k \nabla \cdot (\vec{T})] \quad 3$$

The stress tensor in the momentum expression, $\vec{\tau}$, can be calculated by:

$$\vec{\tau} = \mu \left[(\nabla \vec{v} + \nabla \vec{v}^T) - \frac{2}{3} \nabla \vec{v} \mathbf{I} \right] \quad 4$$

By making these simplifications and expansions, Eqs. 1 and 2 can be rewritten for a steady state as **ANSYS**:

$$\nabla \cdot (\rho \vec{v}) = 0 \quad 5$$

$$\nabla \cdot (\rho \vec{v} \vec{v}) = -\nabla P + \mu (\nabla^2 \cdot \vec{v}) + \rho \vec{g} \quad 6$$

$$\nabla \cdot (\rho c_p \vec{v} \vec{T}) = \nabla \cdot [k \nabla \cdot (\vec{T})] \quad 7$$

The fluid density can be simplified at all points within the employed domain, by employing the Oberbeck-Boussinesq approximation to linearize the temperature dependency of density.

The buoyancy force is redefined as **Ganguli et al., (2009)**:

$$\rho \vec{g} = \vec{g} [\rho_{\text{ref}} - \rho_{\text{ref}} \beta (T - T_f)] = \rho_{\text{ref}} \vec{g} [1 - \beta (T - T_f)] \quad 8$$

Where β represent a fluid compressibility found via:

$$\beta = -\frac{1}{V} \frac{\partial V}{\partial P} \quad 9$$

The air can be considered as an ideal gas at nominal atmospheric pressures and temperatures, the air compressibility found by:

$$\beta = \frac{1}{T_f} \quad 10$$

A necessary simplification was made to the mass and momentum equations present in Eqs. 4 and 5 allows for the development of the final forms for incompressible flow:

$$\nabla \cdot (\vec{v}) = 0 \quad 11$$

$$\vec{v} \cdot (\nabla \cdot \vec{v}) = -\frac{1}{\rho_{\text{ref}}} \nabla P + \nu_{\text{ref}} (\nabla^2 \cdot \vec{v}) + \vec{g} [1 - \beta (T - T_f)] \quad 12$$

2.3. Boundary Conditions

Obstacle Surface: the fluid velocity at the surface of the solid must be zero in all directions:

$$v_x = v_y = 0 \quad 13$$

For adiabatic obstacle boundary condition:

$$\frac{\partial T}{\partial n} = 0 \quad 14$$

Right and left walls: the heat flux is assumed to be constant along the Right and left walls:

$$\frac{\partial T}{\partial n} = \frac{q''}{k_{ref}} \quad 15$$

where n refers to the direction normal to the surface and q'' is the heat flux.

Top and bottom walls: the confining wall is assumed to be adiabatic, signifying a zero temperature gradient normal to the partition surface.

$$\frac{\partial T}{\partial n} = 0 \quad 16$$

Air Inlet: the air inlet with constant velocity and temperature as following:

$$v_y = v_{in} = 0.2, 0.3, 0.4 \text{ and } 0.5, T = T_{in} = 298 \text{ K} \quad 17$$

Air Outlet: The outlet vent, which specify a zero pressure differential normal to the open surface:

$$\frac{\partial P}{\partial n} = 0 \quad 18$$

At the outlet section, the flow and temperature fields are assumed to be fully developed. The outflow boundary condition has been implemented in the outlet section. This boundary condition implies zero normal gradients for all flow variables except pressure. Thus, by using sweeping outlet temperature boundary conditions as:

$$\frac{\partial T}{\partial y} = 0 \quad 19$$

2.4. Grid Independence Test

A grid independence test was performed to evaluate the effects of grid sizes on the results. Four sets of mesh were generated using tetrahedral three dimensional meshes with 15552, 17565, 19225 and 20170 nodes. It was observed that the 19225 and 20170 nodes produce almost approximated identical results with a percentage error of 0.135%. Hence, a domain with 20170 nodes was chosen to increase the computational accuracy. The summary of the grid independence test results is shown in [Table 1](#).

Table 1. Grid independence test results.

Nodes	Outlet temperature (K)	Percentage error (%)
15552	307.2546	1.165
17565	308.4568	0.833
19225	310.0887	0.186
20170	310.6256	0.135

2.5. Computational Grids and Numerical Method

To study the problem of the heat transfer by mixed convection parameters of the air inside a truncated cone enclosure with heated left and right inclined walls and a triangular obstacle in the middle of the enclosure. Also, the finite-volume computational nodes were generated for the present two dimensional enclosure geometry. In an effort to simplify the construction of each of this geometry and mesh files, the Auto-CAD and Gambit v. 2.3.16 software are used. The air space modeled using a quadrilateral mesh by 20170 nodes and Fig. 2 displays an example of this computational domain.

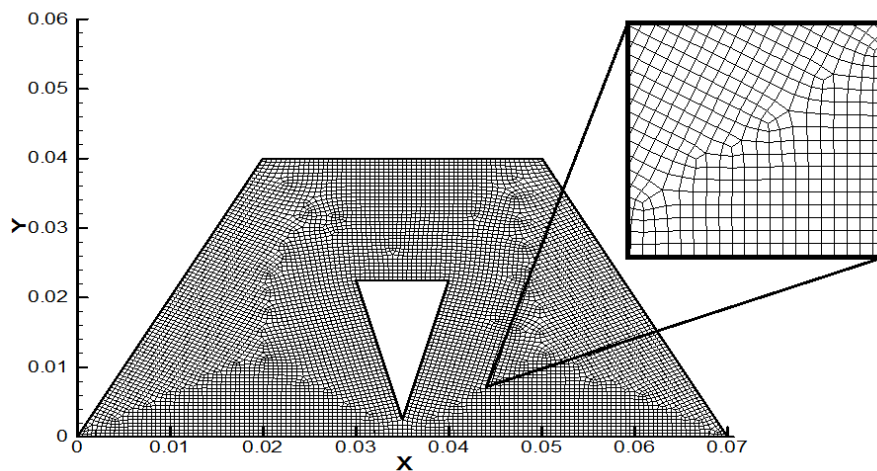


Fig. 2. The two dimensional truncated cone enclosure with aspect ratio.

The 2D computational domain exported to the FLUENT, in this study, to couple the inlet and outlet pressure boundary conditions the SIMPLE algorithm was performed. The simulation iteration was terminated when the mass, momentum, and energy residuals drop below 10^{-9} for each simulation iteration. By using under-relaxation factors of 0.70 and 0.30 for the pressure and momentum equations respectively, but the density and energy relaxation factors were left at the default values of unity.

3. RESULTS AND DISCUSSION

The present numerical work has been presented in mixed convection system where the Richardson number is in the range of $Ri = 7$ to 11 for two different inlet Reynolds number $Re = 600$ to 1600. The mixed convection problem presented in the truncated cone enclosure, top and bottom walls were assumed as adiabatic. In this section, the laminar steady flow results have been achieved. Firstly, the streamline and isotherm contours were presented for different obstacle height varying for six different positions within the geometry ($h = 0$ or without obstacle, 2.5, 5, 7.5, 10, 12.5 and 20 cm (see Fig. (1b)) from the inlet port.

The present calculations were performed at constant $Pr=0.712$ for air [18], and constant position and length of the heated wall of the left and right surfaces of the cone. In addition, its length is about $L_p=45$ cm to simulate a solar container model of truncated cone enclosure geometry. The heated wall with different inclination angles of $\theta= 20^\circ, 30^\circ, 40^\circ, 50^\circ$ and 60° , in order to obtain various aspect ratio in the range of $A= 0.75, 1.75, 2, 2.45$ and 2.65 . At each A , the Reynolds number, Richardson number, Rayleigh number was varied in order to obtain the flow conditions.

3.1. Effect of obstacle Position

In all cases of position of the obstacle chosen in this study the cases of $h=0, 5, 10,$ and 20 presented in Fig. 3 for the same angle of inclination of the legs of the cone. However, the results showed that the presence of the obstacle in the way of the inlet air flow will increase the temperatures contour values near the heated walls. Furthermore, it makes a thermal stratified zone on the upper region of the triangular obstacle due to redirection the air flow toward the heated left and right walls instead of the upper wall in order to extract the heat to the bottom port. But, when changing the obstacle position toward the top wall leads to increasing the air flow distance that the researchers observed that the temperatures near the heated wall decreased, and appeared the circulation region near the heated zone. Also, the results showed that the thermal stratified zone upper the obstacle start decreasing until it disappeared gradually in the case of $h=20$ cm.

The effect of changing the position of the triangular obstacle on the air flow streamlines, shown in Fig. 4. It displayed the streamlines inside the truncated cone cavity with obstacle height 0 to 20 cm. The results showed that increasing the obstacle height will increase the air circulation near the heated walls. The buoyancy force direction and momentum force identical along the source heated surfaces at $h=20$ cm and $h=5$ cm. Long vortices appeared in the region below the mainstream. The mainstream viscous forces drive rotating eddy against the buoyancy force at the heated surfaces. These two positions delimit the possible minimum and maximum heat transfer. Basically, the interaction of the main stream flow and heated surfaces flow increased by using a triangular obstacle and by increasing its height. Where the main flow attached to the heated wall but the eddies that generated by the viscous driven cause a heated walls which is driven the heated buoyancy force. This effect can be observed clearly in the case of plotting the y-direction velocity vector in Fig. 5 plotted the dynamic field for different buoyancy ratio values and can show the vortices intensity increased by increasing

the obstacle height. The fluid falls downward from the upper region and the flow divided into two small cells turning from the center to the cold sides.

3.2. Effect of enclosure angle

The effect of increasing the enclosure inclination angles on the isothermal lines is plotted in Fig. 6. The results show that increasing inclination angles lead to decrease the thermal layers near the heated walls due to transfer the walls from inclined to vertical position and decreasing the buoyancy ratio values near the heated walls. Also, the increasing angles will decrease the temperature upper the obstacle. For a various enclosure shape that caused by various titled angles, the streamline were plotted, as shown in Fig. 7. The results obtained for a constant $Ra=2.36 \times 10^7$, Richardson number $Ri=11$, Reynolds number $Re=1600$, and obstacle position $h=7.5$ cm. The results show that there are no significant changes in the streamlines between the obstacle height and the heated walls. If the cavity size is increased strongly there is a small effect on the streamlines in the area above the obstacle. In the zone between heated walls and the outlet port which show that the flow affected by the enclosure inclination angle.

3.3. Effect of Rayleigh number and Reynolds number

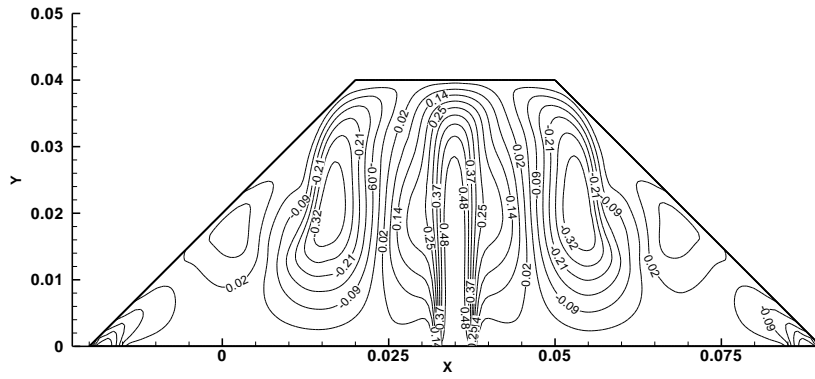
Fig. 8 and Fig. 9 presented the results of the isothermal and streamline respectively at $h=5.0$ cm, inclination angle fixed at $\theta=60^\circ$ and Richardson number at $Ri = 11$. And varied the Rayleigh number from $Ra = 1.57 \times 10^6$ to $Ra = 7.9 \times 10^8$, and varied the inlet Reynolds number from 600 to 1300 the results show the increasing Rayleigh number will increase the temperature distribution between the obstacle and the heated surface. The Figs. also show that increasing the Reynolds number lead to increase the streamlines above the obstacle region. And show that the secondary flow (flow induced by the heated surface) increased when using the low Reynolds number such as $Re=600$ and 1000 as compared with the main flow (flow induced by the inlet velocity), but when increasing the Reynolds number up to 1000 show that the secondary flow will disappear gradually at Reynolds number 1600 .

Fig. 10 and Fig. 11 showed the velocity profile in term of obstacle height and enclosure angles of inclination respectively. The figures show that the increasing the obstacle height from 0 to 20 cm lead to increase the velocity profile between the obstacle and the heated surfaces. But, when increasing the inclination angles it was shown that the velocity in the region between the obstacle and the heated surface is increased too.

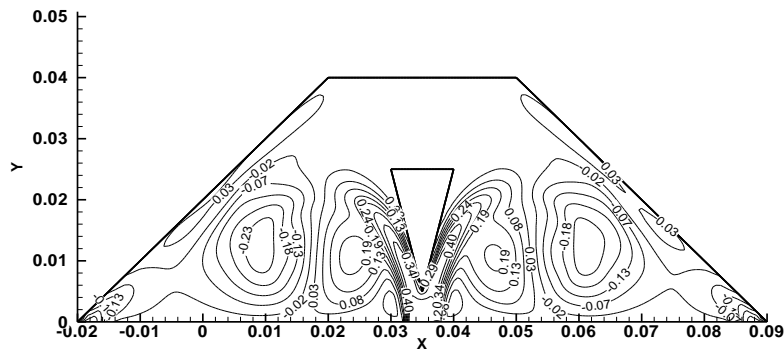
3.4. Local and overall Nusselt number

The local Nusselt number Nu along the right side of the enclosure is presented in Fig. 12. It shows also a dependence of the source power of the heated wall for high Reynolds number $Re=1600$, however, it differs from the behavior of the $Nu_{overall}$. Cavity with obstacle of $h=7.5\text{cm}$ performed maximum heat transfer. The main flow is directed to the cavity surfaces by the heated walls itself where this develops the convection at the enclosure walls. The results show that the local Nusselt number (Nu) increased with increasing the heat flux and decreased with percent by 76 % as transferred from the top to the bottom location of the heated wall at $Ra=2.36\times 10^7$. However, Fig. 13 shows the dependence of the local Nusselt number on the Reynolds numbers. It is clearly shown that the Nusselt number increased with increasing the Reynolds number from 1000 to 1600 but the maximum Nusselt number found in Reynolds number from 600 about $Nu=35$ in the region between the obstacle and the heated right wall.

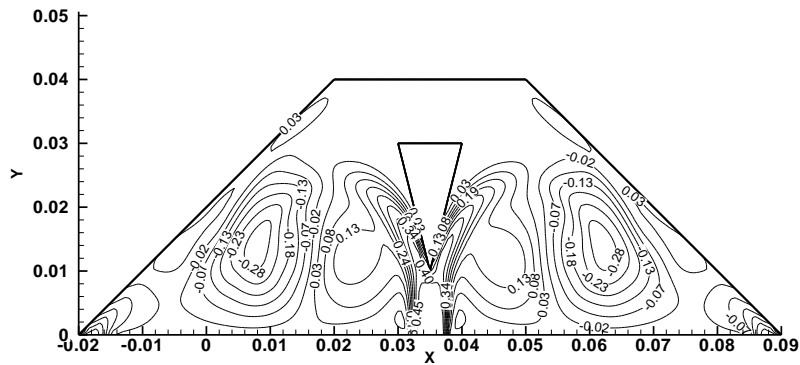
For high Re , the main flow inside the cavity takes apart from the secondary flow. The two flows (main flow and secondary flow) do not interact for positions like $h=0$ to 20 cm. However, the convective fluid flow from the inlet to the outlet port stays at low temperature lead to very high cavity Nu in Fig. 14. Moreover, the cavity Nu increases with increasing the height of the obstacle toward the upper region of the enclosure but decreasing in the lower region. Fig. 15 presented the effect of the cone legs titled angle on the local Nu . The obstacle position remains constant at $h=7.5$ cm. The results show that the increasing in the inclination angle will lead to increase the maximum value of the local Nusselt number from 25 to 36 when increased the inclination angle from 20° to 60° . The overall Nu and the cone cavity Nu are used to present the heat transfer from the heated right wall as presented in Fig. 16. The results show that the overall Nusselt number increases upon increasing the Reynolds number and with increasing the obstacle position $\theta=20^\circ$, $Ri=11$, $Ra=2.36\times 10^7$. The overall Nusselt number increased by 20% when using obstacle at a position of $h=5$ cm. The inlet Re has the sufficient effect on all studied parameters. There is a considered enhancement of the convective heat transfer that can be achieved with varying the obstacle height. But in case of using Richardson number as presented in Fig. 17, it was shown that the overall Nusselt number increased with increasing the Richardson number only case of $h=0$ and 5 cm but for cases of above 5 cm show that Nusselt number decreased with increasing the Richardson number.



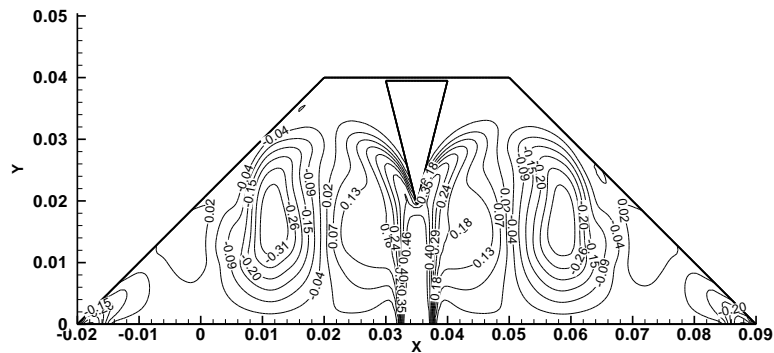
a) $h=0.0$ cm



b) $h=5.0$



c) $h=10$ cm



d) $h=20$ cm

Fig. 4. Streamlines at air flow at $\theta=20^\circ$, $Re = 1600$, $Ri = 11$, $Ra=2.36 \times 10^7$.

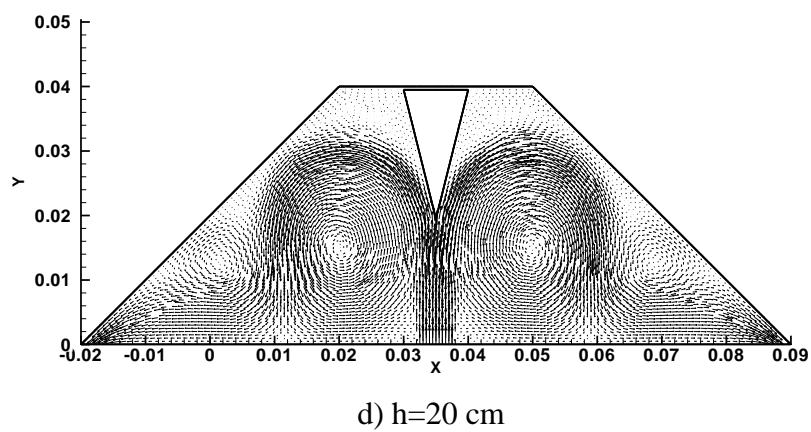
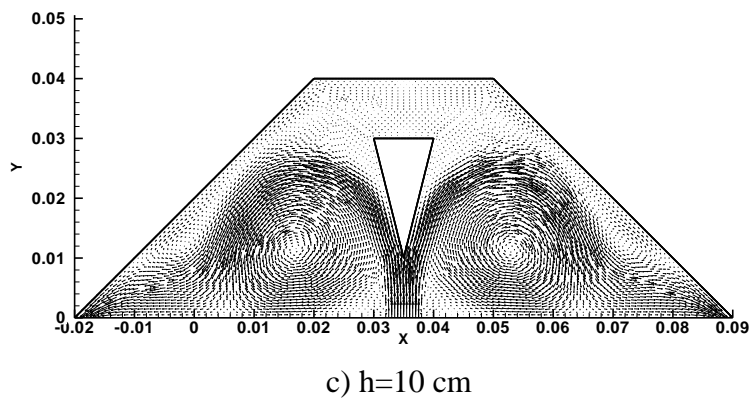
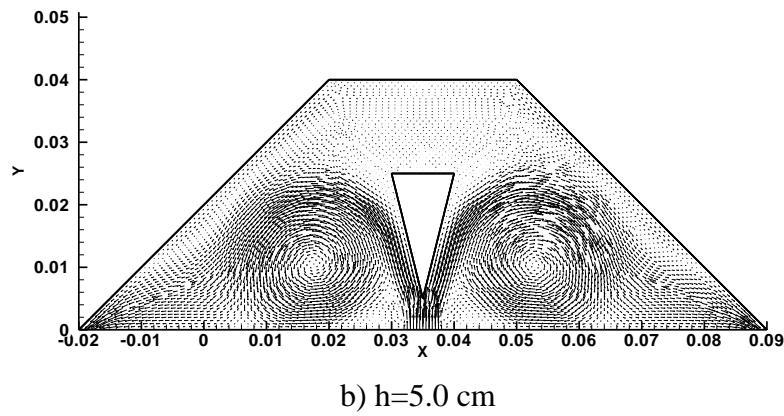
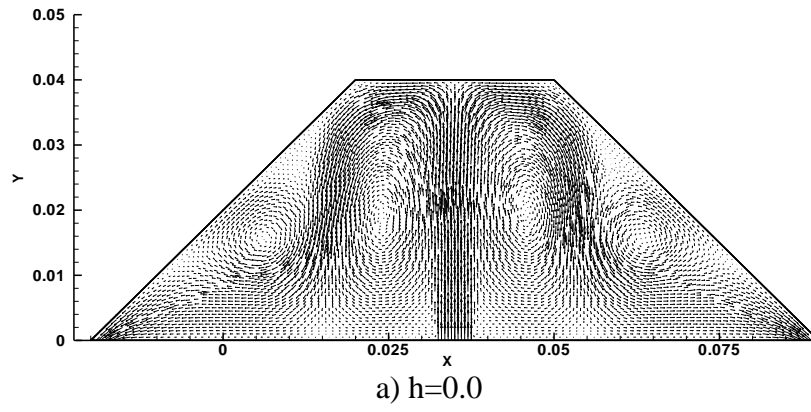
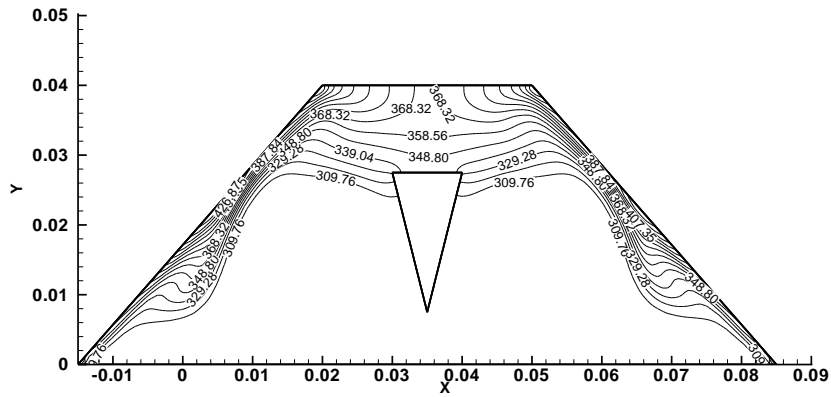
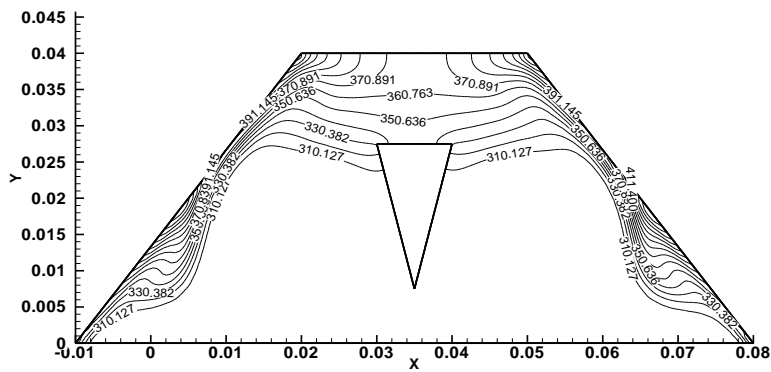


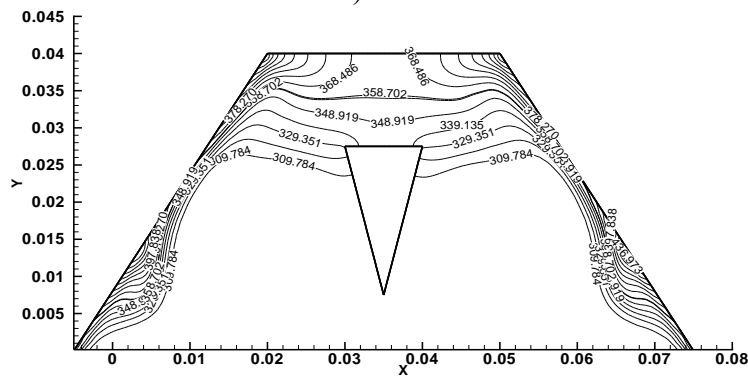
Fig. 5. Velocity vector for air flow at $\theta=20^\circ$, $Re = 1600$, $Ri = 11$, $Ra=2.36 \times 10^7$.



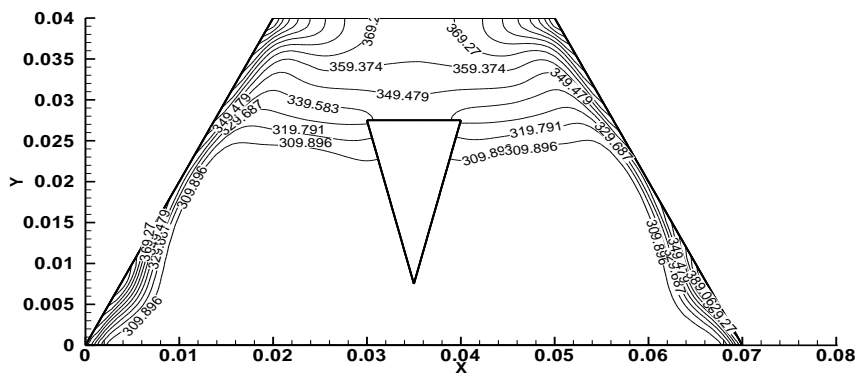
a) $\theta=30^\circ$



b) $\theta=40^\circ$

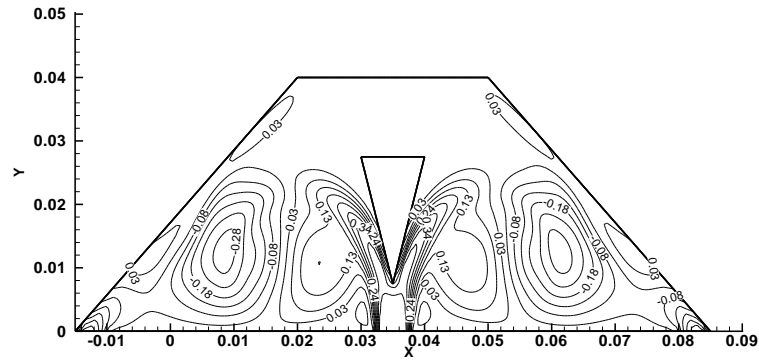


c) $\theta=50^\circ$

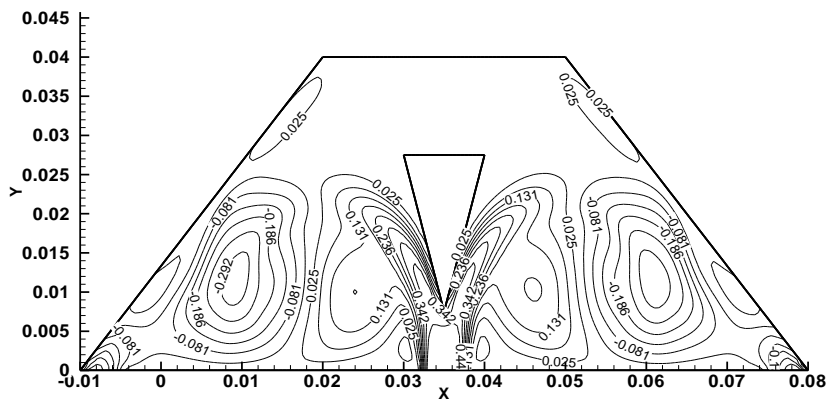


d) $\theta=60^\circ$

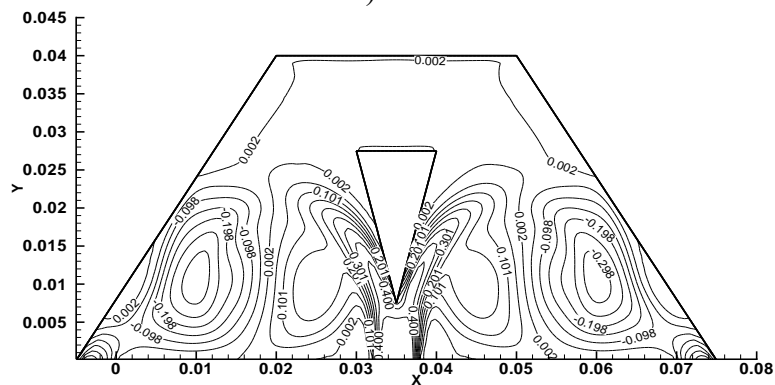
Fig. 6. Isothermal lines at air flow at $h=7.5\text{cm}$, $Re = 1600$, $Ri = 11$, $Ra=2.36 \times 10^7$.

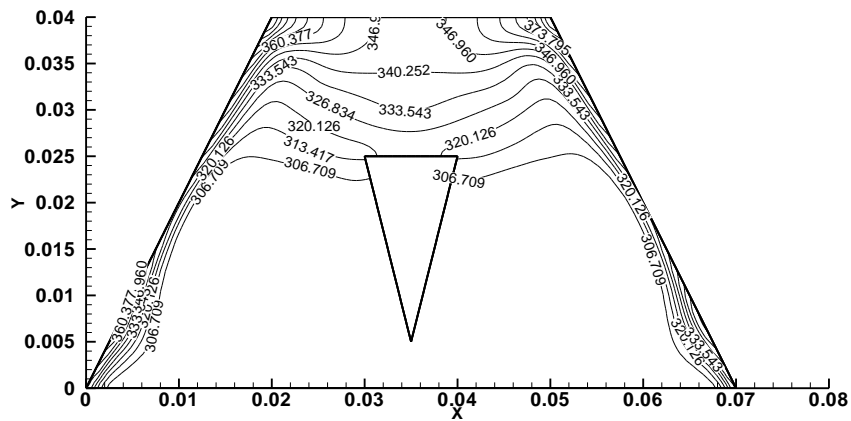


a) $\theta=30^\circ$

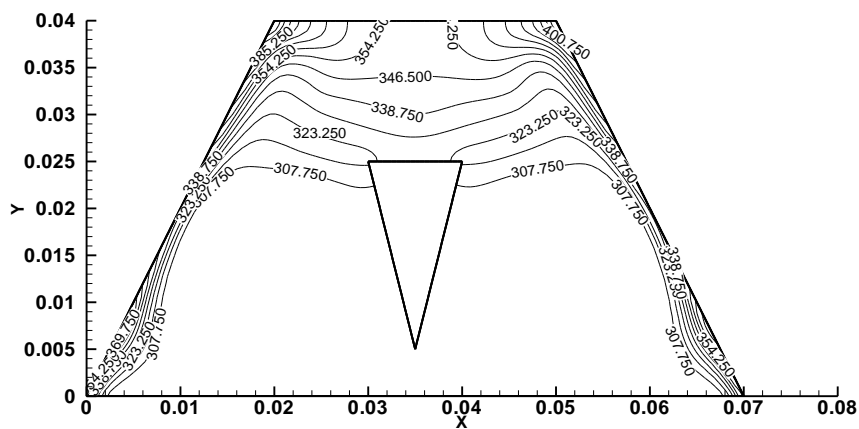


b) $\theta=40^\circ$

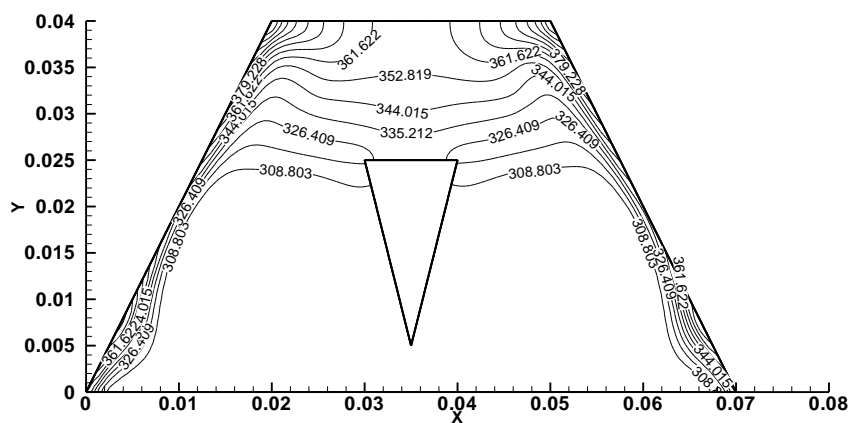




a) $Ra = 1.57E+06$



b) $Ra = 1.57E+07$



c) $Ra = 1.57E+08$

Fig. 8. Isothermal lines for air flow at $h=5.0$ cm, $\theta=60^\circ$, $Re = 1600$, $Ri = 11$.

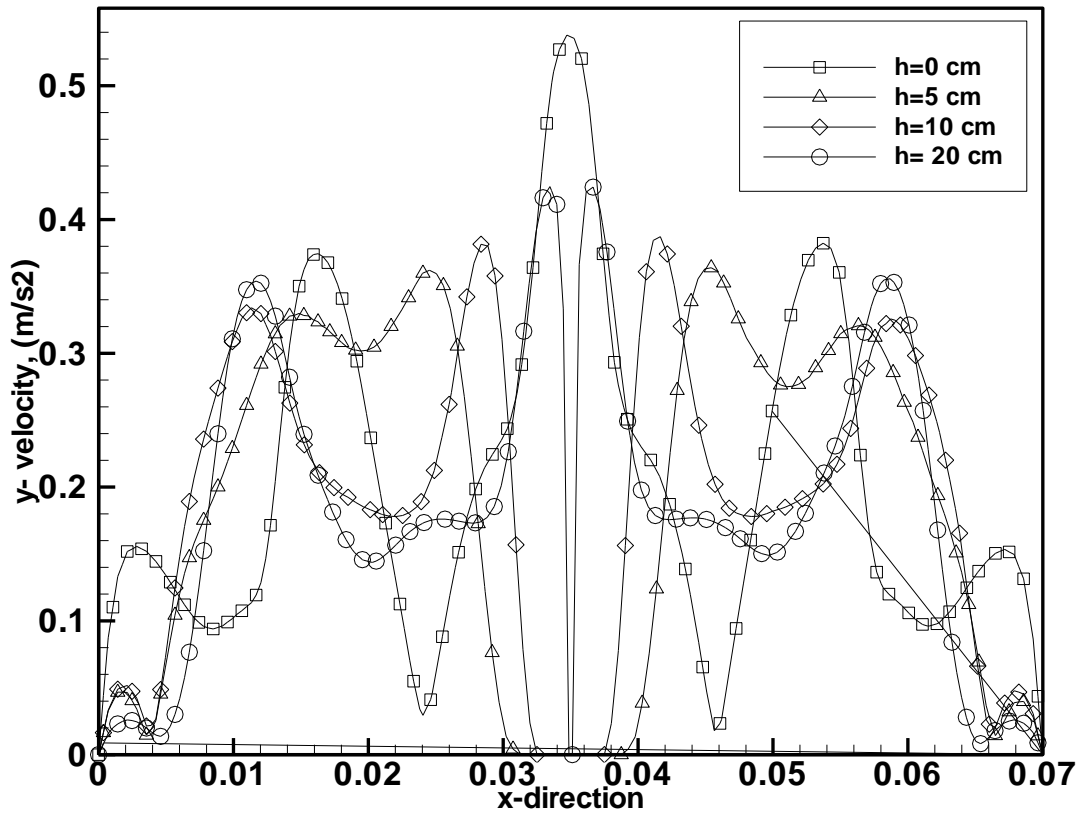


Fig. 10. velocity centerline of the enclosure for different of the obstacle position at $\theta=60^\circ, h=5.0\text{cm}, Re=1600, Ra=2.36 \times 10^7$.

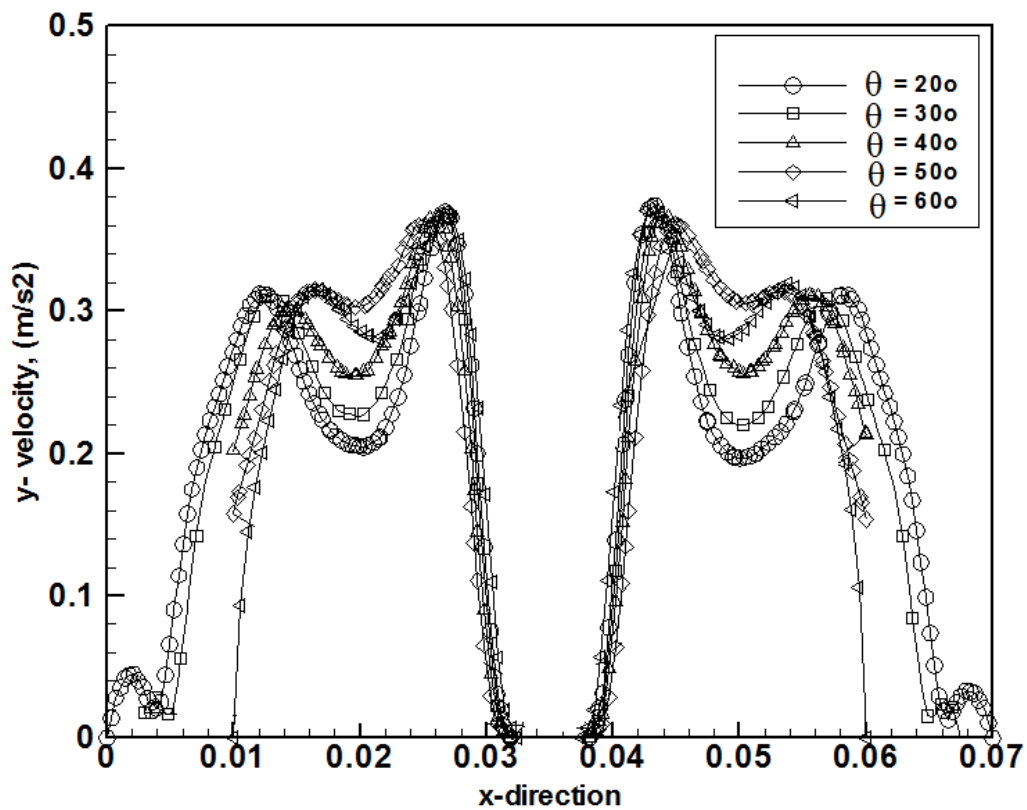


Fig. 11. velocity centerline of the enclosure for different of the obstacle position a $h=5.0\text{cm}, Re=1600, Ra=2.36 \times 10^7$.

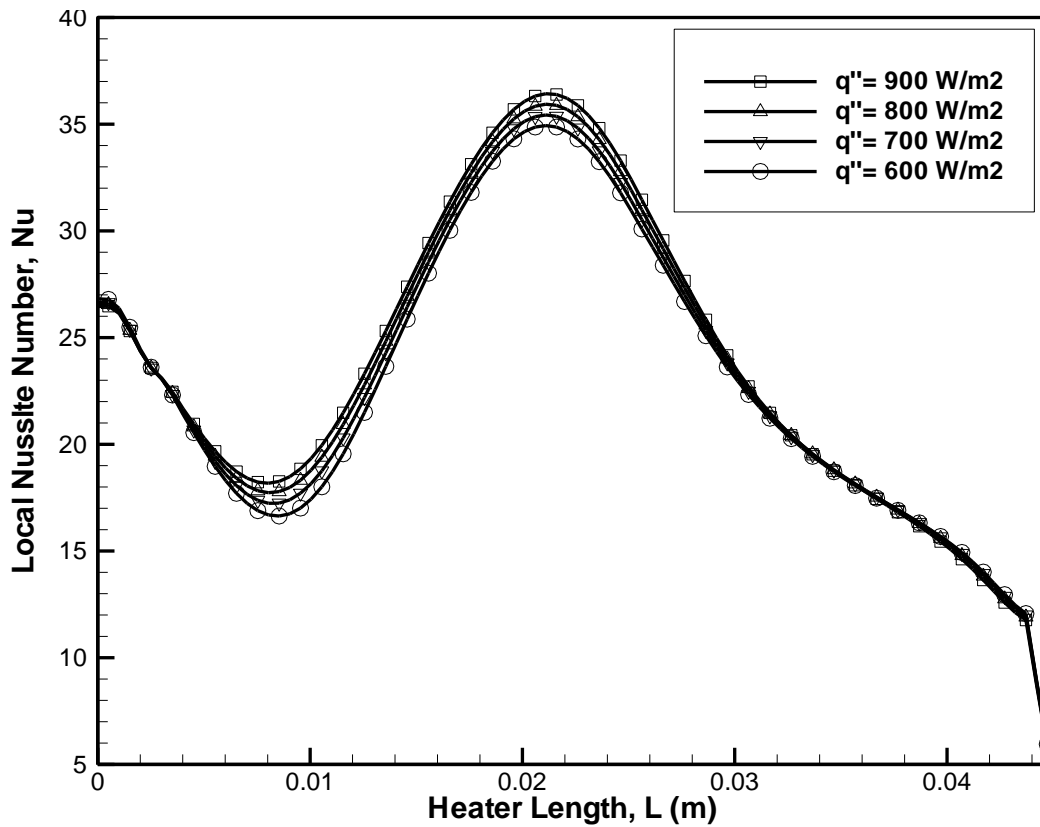


Fig. 12. Enclosure Local Nusselt number independence of the left heater length for different of the heat source at $\theta=20^\circ, h=7.5\text{cm}, Re=1600, Ra=2.36 \times 10^7$.

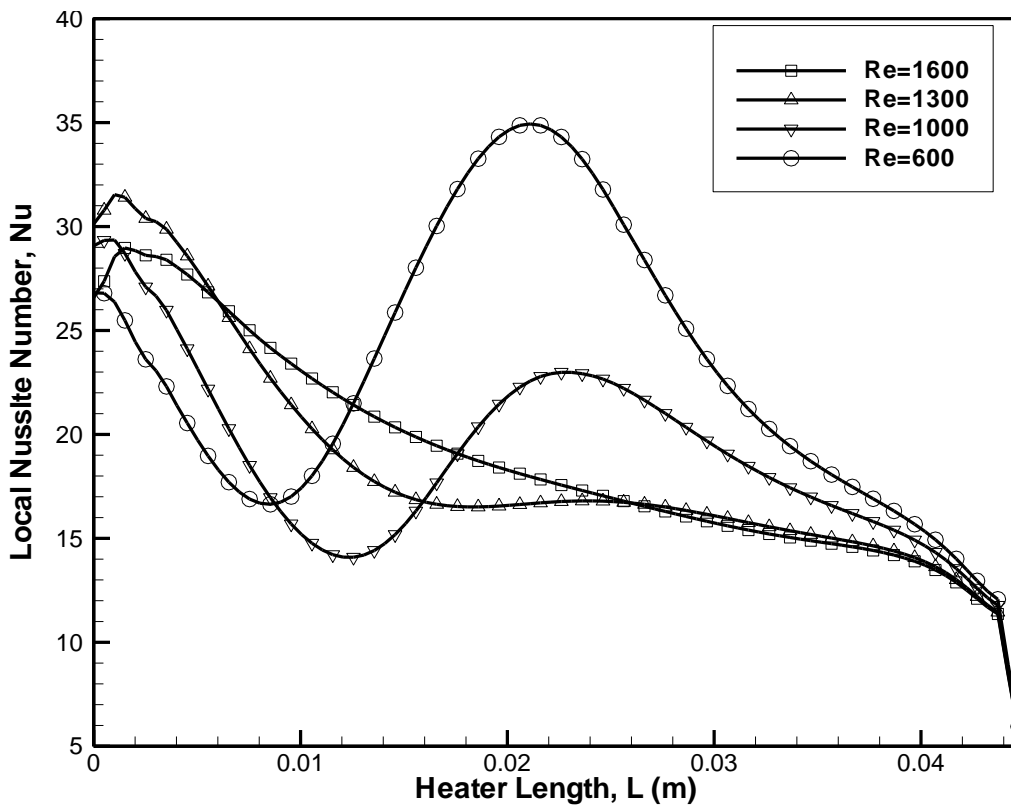


Fig. 13. Enclosure Local Nusselt number independence of the left heater length for different Reynolds number for, $\theta=20^\circ, h=7.5 \text{ cm}, Ri=11, Ra=2.36 \times 10^7$.

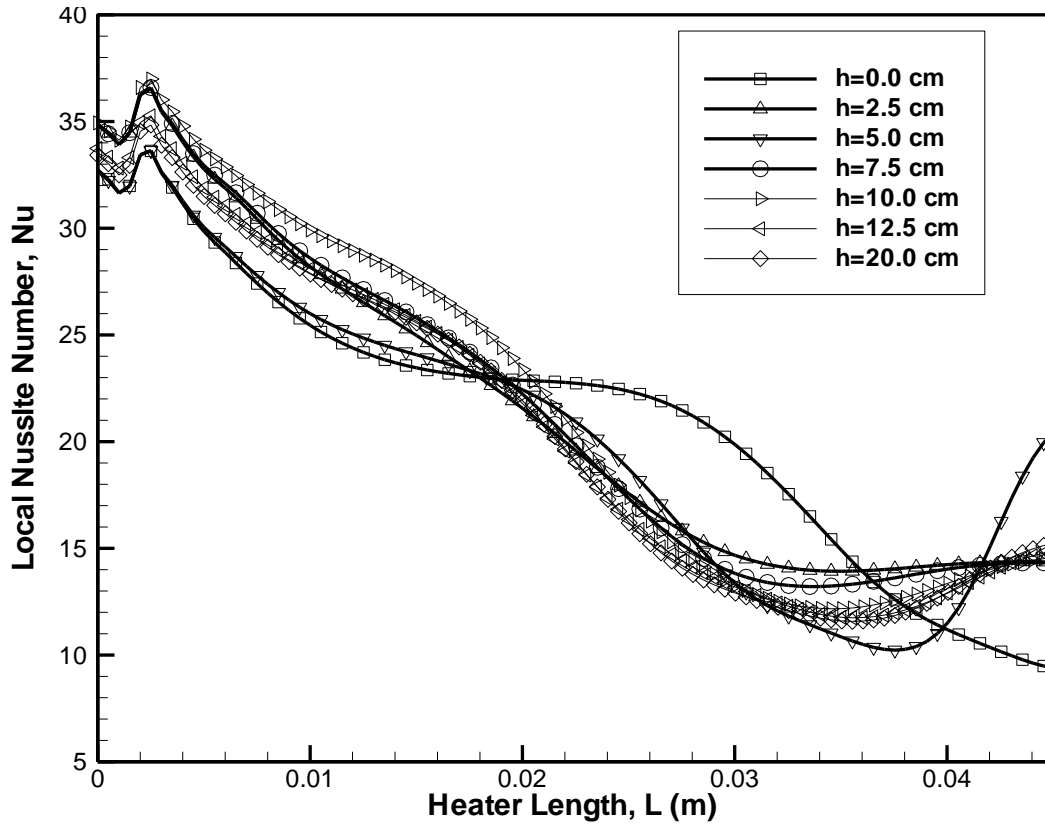


Fig. 14. Enclosure Local Nusselt number independence of the left heater length for different obstacle position for, $Re=1600$, $\theta=20^\circ$, $Ri=11$, $Ra=2.36 \times 10^7$.

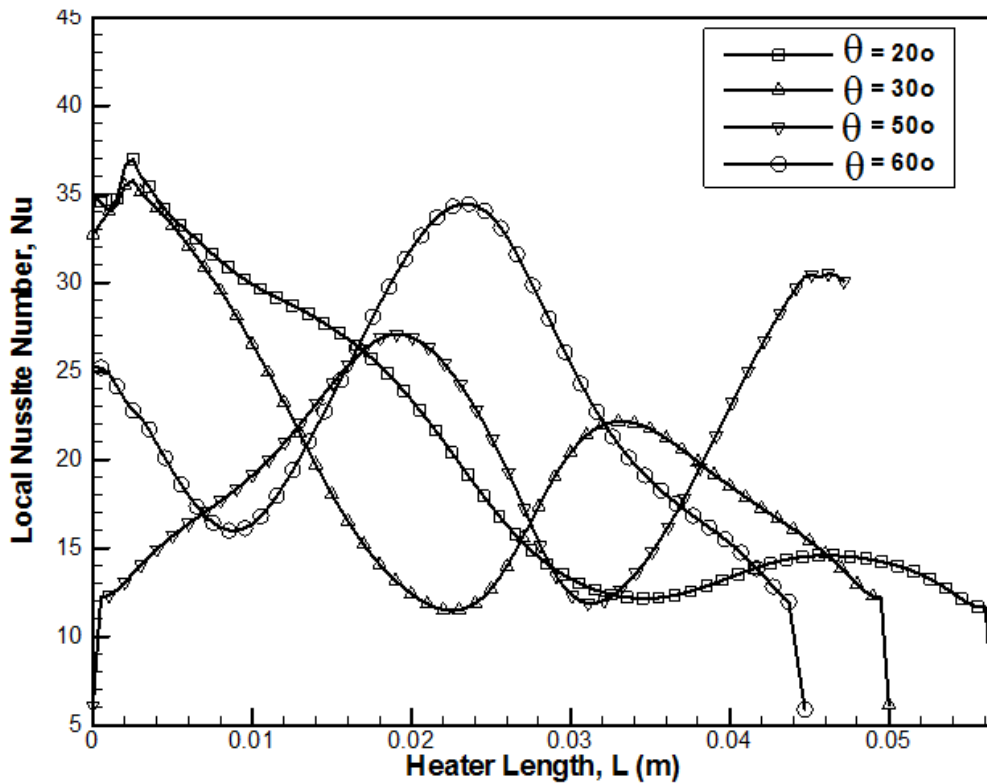


Fig. 15. Enclosure Local Nusselt number independence of the left heater length for different inclination angle for, $h=7.5$ cm, $Ri=11$, $Ra=2.36 \times 10^7$.

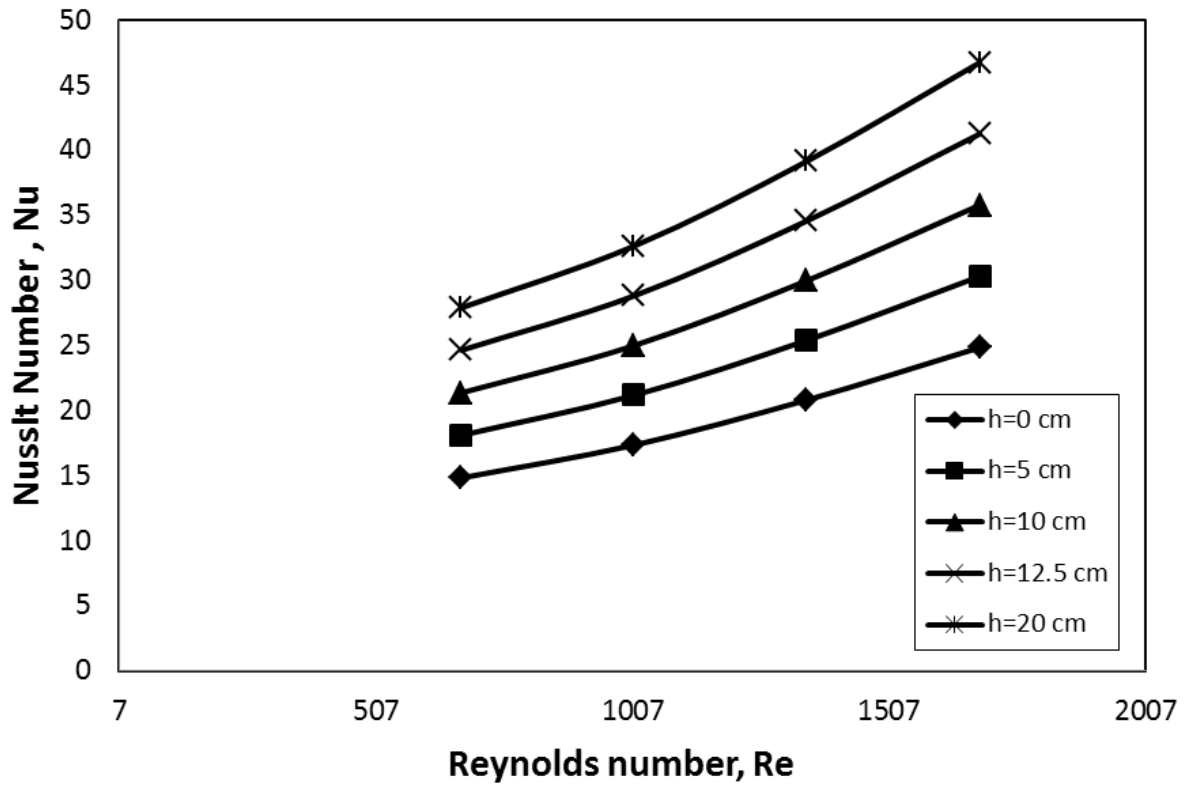


Fig. 16. Effect of obstacle height on overall Nusselt number for Richardson number, $\theta=20\circ$, $Ri=11$, $Ra=2.36 \times 10^7$.

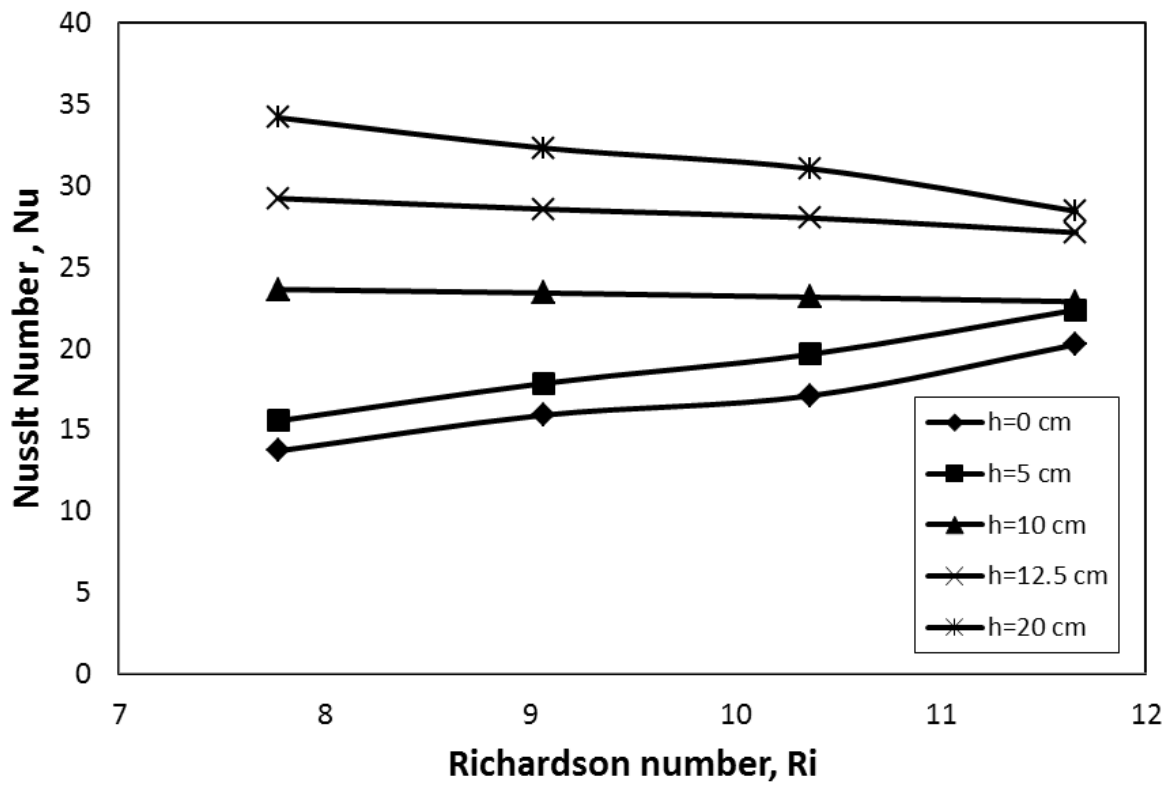


Fig. 17. Effect of obstacle height on overall Nusselt number for Richardson number, $Re=1600$, $\theta=20\circ$, $Ri=11$, $Ra=2.36 \times 10^7$.

4. CONCLUSIONS

This study emphasized on the mixed convection heat transfer of a suggested solar container with subjected heat flux on the inclined right and left walls with different angles of inclination. The forced flow of one inlet with different values of the Reynolds number and two outlet ports is thermally coupled. The results of streamline and isothermal give a good indication up on the air thermal and flow distribution inside the enclosure for all conditions employed. The mixed convection heat transfer is presented by the local and overall Nu. The effect of Reynolds number, the Richardson number, the heat flux in addition to the cavity specification such as the triangular obstacle height, cone legs title angles and aspect ratio are studied in this work. The present numerical results show that the Nu increases with increasing the inlet Re, with increasing the triangular obstacle positions. On the other hand, by increasing the cone titled angles in the case that the cavity area is maximized yields a rise of the overall Nu where natural and forced convection compete.

5. REFERENCES

Alamgir, M., Overall heat transfer from vertical cones in laminar free convection: an approximate method, *ASME Journal of Heat Transfer*, 101, pp. 174–176, 1989.

ANSYS Academic Research CFD version 12 user guide & Manuals.

Aounallah M., Y. Addad and S. Benhamadouche and O. Imine and L. Adjlout and D. Laurence, “Numerical investigation of turbulent natural convection in an inclined square cavity with a hot wavy wall, *International Journal of Heat and Mass Transfer*, vol. 50, pp. 1683–1693, 2007.

Bapuji Pullepu, K. Ekambavanan, A. J. Chamkha, 2008, Unsteady Laminar Free Convection from a Vertical Cone with Uniform Surface Heat Flux, *Nonlinear Analysis: Modelling and Control*, 2008, Vol. 13, No. 1, 47–60.

Dixit, HN., and V. Babu, Simulation of high Rayleigh number natural convection in a square cavity using the lattice Boltzmann method, *International Journal of Heat and Mass Transfer*, vol. 49, pp. 727–739, 2006.

Elsayed M. A. Elbashbeshy, Tarek G. Emam, and Emad A. Sayed, 2016, Effect of Thermal Radiation on Free Convection Flow and Heat Transfer Over a Truncated Cone in Presence of Pressure Work and Heat Generation/Absorption, *Thermal Science*, Year 2016, Vol. 20, No. 2, pp. 555-565

Fuad E., Kent and E. Asmaz and S. Ozerbay, Laminar natural convection in right triangular enclosures, *Heat and Mass Transfer*, 2007, Vol. 44, pp. 187–200.

Ganguli, A.A., A.B. Pandit and J.B. Joshi, CFD simulation of heat transfer in a two-dimensional vertical enclosure,” *Chemical Engineering Research and Design*, vol. 87, pp. 711–727, 2009.

He Y.L., W.W. Yang and W.Q. Tao, “Three-Dimensional Numerical Study of Natural Convective Heat Transfer of Liquid in a Cubic Enclosure,” *Numerical Heat Transfer Part A Applications*, vol. 47, pp.917-934, 2005.

Hossain, M.A., S.C. Paul, Free convection from a vertical permeable circular cone with nonuniform surface temperature, *Acta Mechanica*, 151, pp. 103–114, 2001.

Jan Langebach, Peter Fischer, and Christian Karcher, 2007, Convective Heat Transfer of Internal Electronic Components in a Headlight Geometry, *PWASET VOLUME 22 JULY 2007 ISSN 1307-6884*.

Merk, H. J., J.A. Prins, Thermal convection laminar boundary layer I, *Appl. Sci. Res. A*, 4, pp. 11–24, 1953.

Merk, H. J., J.A. Prins, Thermal convection laminar boundary layer II, *Appl. Sci. Res. A*, 4, pp. 195–206, 1954.

Papanicolaou, E., Y., Jaluria, computation of turbulent flow in mixed convection in a cavity with a localized heat source, *J. Heat Transfer*, vol. 117, pp. 649–658, 1995.

Pop, I., H. S. Takhar, Compressibility effects in laminar free convection from a vertical cone, *Applied Scientific Research*, 48, pp. 71–82, 1991.

Ramanaiah, G., V. Kumaran, Natural convection about a permeable cone and a cylinder subjected to radiation boundary condition, *Int. J. Eng. Sci.*, 30, pp. 693–699, 1992.

Sridhar A., and K.S. Reddy, Transient analysis of modified cuboid solar integrated-collector-storage system, *Applied Thermal Engineering*, vol. 27, pp.330-346, 2007.

Varol Y., and H.F. Oztop and I. Pop, Natural convection in right-angle porous trapezoidal enclosure partially cooled from inclined wall, *International Communications in Heat and Mass Transfer*, , vol. 36, pp.6–15, 2009.

Wang S.G., and T.Y. Li and P.T. Hsu and Kaohsiung and Taiwan, "Natural convection of micropolar fluid in a partially divided enclosure," *Acta Mechanica*, vol. 136, pp. 41 – 53, 1999.